Journal of Alloys and Compounds 473 (2009) 107–115

Contents lists available at ScienceDirect

Journal of Alloys and Compounds

journal homepage: www.elsevier.com/locate/jallcom

Effects of processing parameters on consolidation and microstructure of W–Cu components by DMLS

Dongdong Gu*, Yifu Shen

College of Materials Science and Technology, Nanjing University of Aeronautics and Astronautics, 29 Yudao Street, Nanjing 210016, PR China

ARTICLE INFO

Article history:
Received 2 March 2008
Received in revised form 15 May 2008
Accepted 15 May 2008
Available online 30 June 2008

Keywords:
Metals and alloys
Laser processing
Sintering
Microstructure

ABSTRACT

The densification behavior and attendant microstructural characteristics of direct laser sintered submicron W–Cu/micron Cu powder system under different processing conditions were investigated in this work. The methods for improving the controllability of laser processing were elucidated. A "linear energy density (LED)", which was defined by the ratio of laser power to scan speed, was used to tailor the powder melting mechanisms. It showed that using a suitable LED between ~13 and ~19 kJ/m combined with a scan speed less than 0.06 m/s led to a continuous melting of the Cu component, yielding a sound densification larger than 92% theoretical density without any balling phenomena. With a favorable sintering mechanism prevailed, a proper increase in the LED above ~13 kJ/m, which was realized by increasing laser power or lowering scan speed, produced a homogeneous microstructure consisting of a novel W-rim/Cu-core structure. Narrowing the scan line spacing to 0.15 mm was able to enhance the inter-track bonding, and to reduce the roughness of laser sintered surface. Decreasing the powder layer thickness to 0.15 mm was a promising approach for improving the inter-layer bonding coherence. A "volumetric energy density (VED)" was defined to facilitate the integrated process control by considering the combined effect of various processing parameters. It was found that setting the VED within ~0.6 and ~0.8 kJ/mm^3 favored a better yield of high-density sintered parts.

1. Introduction

Due to a unique combination of high electrical and thermal conductivity of copper and low coefficient of thermal expansion (CTE) and high hardness of tungsten, tungsten–copper (W–Cu) composites have been widely used for thermal and electrical applications such as heavy-duty electronic contacts and heat sink materials for high-power microelectronic devices [1–5].

W–Cu composites are commonly produced by infiltrating porous sintered W with liquid Cu or powder metallurgy (PM) techniques. However, for the infiltration method, there exist a series of process defects such as porosity, copper lakes, and tungsten agglomerates [6]. Additionally, there is a limit to the copper content of 30 wt.% if using this method [7]. In the case of PM method, a significant technological problem is the resultant porosity, due to the mutual insolubility between W and Cu. Furthermore, almost all PM-processed pieces are required to be pre-worked by some dedicated tools (e.g., moulds or dies) to obtain a desired shape. However, because of the limitation of currently available tools, some complex-shaped W–Cu objects are always difficult to be produced.

To overcome these shortcomings, a new fabrication technique, i.e., direct metal laser sintering (DMLS), has been introduced for the production of W–Cu components [8]. DMLS is a laser-based rapid prototyping (RP) technology that builds objects in a layer-by-layer fashion using a bed of loose powder and a computer controlled laser beam [9–16]. DMLS, due to its flexibility in materials and shapes, allows complex three-dimensional (3D) W–Cu objects to be produced without any tools.

However, a review of existing literature reveals that not much previous work has focused on the basic principles of the fabrication of W–Cu components using DMLS. Actually, because of the complex nature of DMLS, which involves multiple modes of heat, mass, and momentum transfer [11,12], process defects associated with DMLS such as balling, curling, and delamination are still difficult to be eliminated completely. It has been found that both powder characteristics (e.g., particle shape, size and its distribution, and component ratio) and processing parameters (e.g., laser power, scan speed, scan line spacing, and powder layer thickness) influence the densification level and the attendant microstructures of DMLS-processed materials [17]. In our previous work [8], we have

* Corresponding author. Tel.: +86 25 52112904x80517; fax: +86 25 52112626.
E-mail addresses: dongdonggu@nuaa.edu.cn, dongdonggu@hotmail.com (D. Gu).

0925-8388/$ – see front matter © 2008 Elsevier B.V. All rights reserved.
doi:10.1016/j.jallcom.2008.05.065

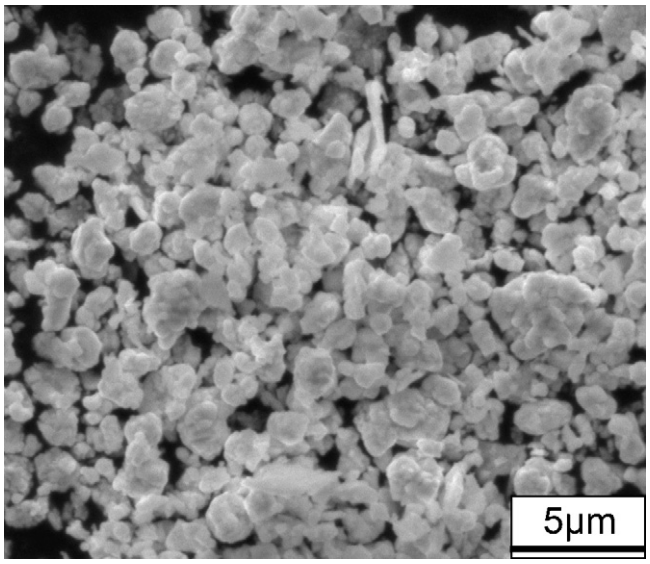

Fig. 1. SEM image showing characteristic morphology of ball-milled powder system.

reported the influence of Cu elemental content on the microstructural evolution and densification response of direct laser sintered W–Cu composites. A sound sintered density accompanied by an interesting W-rim/Cu-core structure has been obtained at a suitable Cu content. Besides the optimization of material characteristics, the possibility of controlling processing parameters in improving the properties of laser sintered W–Cu components is becoming another important consideration. This article presents the sintering mechanisms, surface morphologies, and microstructural features of DMLS-processed W–Cu composites using a wide range of processing parameters, with an aim to elucidate the optimal processing conditions and the relevant control methods.

2. Experimental procedure

2.1. Powder preparation

Electrolytic 99% purity Cu powder with an irregular shape and a mean particle size of 15 μm and submicron W–20Cu (wt.%) composite powder with an irregular morphology and an average particle size of 0.24 μm were used in the current study. The W–20Cu powder was synthesized via combining spray drying and hydrogen reduction [18]. The two powder components were mixed in a Fritsch Pulverisette 6 planetary mono-mill at a rotation speed of 350 rpm for 60 min, with a ball-to-powder weight ratio of 10:1. A homogeneous W–Cu powder system was obtained after mechanical milling, as shown in Fig. 1. Using such a bimodal-sized powder bed was able to improve the flowability of the powder mixture while keeping a fine structure of W in the system.

2.2. Laser processing

The used DMLS system mainly consisted of a continuous wave Gaussian CO_2 laser with a maximum output power of 2000 W, an automatic powder delivery system, and a computer system for process control.

Single layer sintering tests were performed in ambient atmosphere by repeated scanning a powder layer (0.15 mm in thickness) on a Q235 steel substrate using a simple linear raster scan pattern. From these experiments, a series of typical processing parameters were chosen for further preparation of 3D samples with dimensions of 40 mm × 15 mm × 6 mm. Further details regarding DMLS process can be found in the literature [19,20]. The used processing parameters were: spot size 0.30 mm, laser power 300–1200 W, scan speed 0.02–0.08 m/s, scan line spacing 0.15–0.30 mm, and powder layer thickness 0.10–0.30 mm.

2.3. Characterization

Photographs of the real-time laser sintering process were recorded using a SONY DSC-P8 digital camera. Densities of laser sintered samples were calculated based on Archimedes' law. Specimens for metallographic examinations were cut, ground, and polished according to standard procedures. No etching was performed. Surface morphologies and microstructural features of specimens were characterized using a Quanta 200 scanning electron microscope (SEM) at an accelerating voltage of 20 kV. An EDAX energy dispersive X-ray spectroscope (EDX) was used to determine chemical compositions.

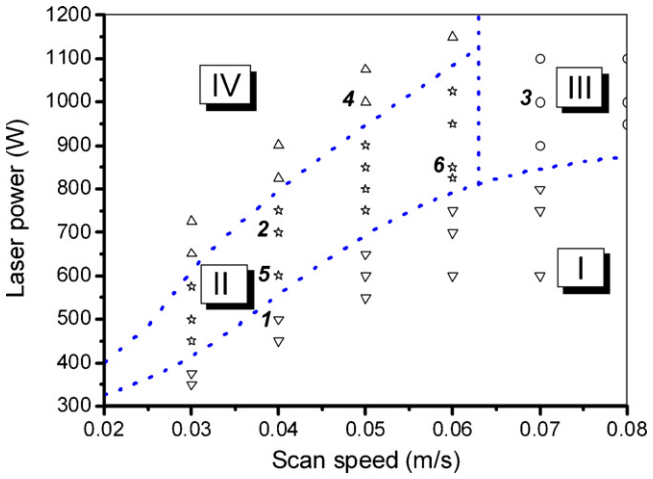

Fig. 2. Mechanisms of single layer melting processed over a wide range of laser powers and scan speeds for the W–Cu system. Laser sintering using "▽" denoted parameters results in slight melting; laser sintering using "☆" denoted parameters leads to continuous melting; laser sintering using "○" denoted parameters results in melting with balling; laser sintering using "△" denoted parameters results in melting with breakage.

3. Results

3.1. Mechanisms of powder melting

Fig. 2 depicts the process map regarding the change of mechanisms of single layer melting. Over the entire range of laser powers and scan speeds, the following four process windows can be defined:

(I) *Slight melting*. The incident laser energy was great enough to exert an effect on the powder bed, but insufficient to induce any significant melting of the powder.
(II) *Continuous melting*. The delivered energy produced continuous molten tracks by means of the complete melting of the Cu component, leading to coherent sintered tracks after solidification.
(III) *Melting with balling*. Using a high laser power and a high scan speed (>0.06 m/s) resulted in the formation of liquid scan tracks of a long thin cylindrical shape, which then broke up into a series of metallic spheres as a consequence of surface tension reduction.
(IV) *Melting with breakage*. At a high laser power combined with a low scan speed (<0.06 m/s), the localized heat input and the attendant heat affected zone around the molten pool were enhanced considerably. The molten scan tracks broke up at longer intervals due to the excessive shrinkage during liquid–solid transition, forming the interrupted sintered tracks on cooling.

It should be noted that the process map is defined based on a series of points, which are indicated by different symbols in Fig. 2. In each process window, laser sintering using the processing parameters within it yielded a similar mechanism of melting. With these key pointes determined, the boundaries between the four different windows were drawn approximatively. The boundary locations were not absolutely strict, due to the span of parameters choice (typically 50 W for the laser power and 0.01 m/s for the scan speed).

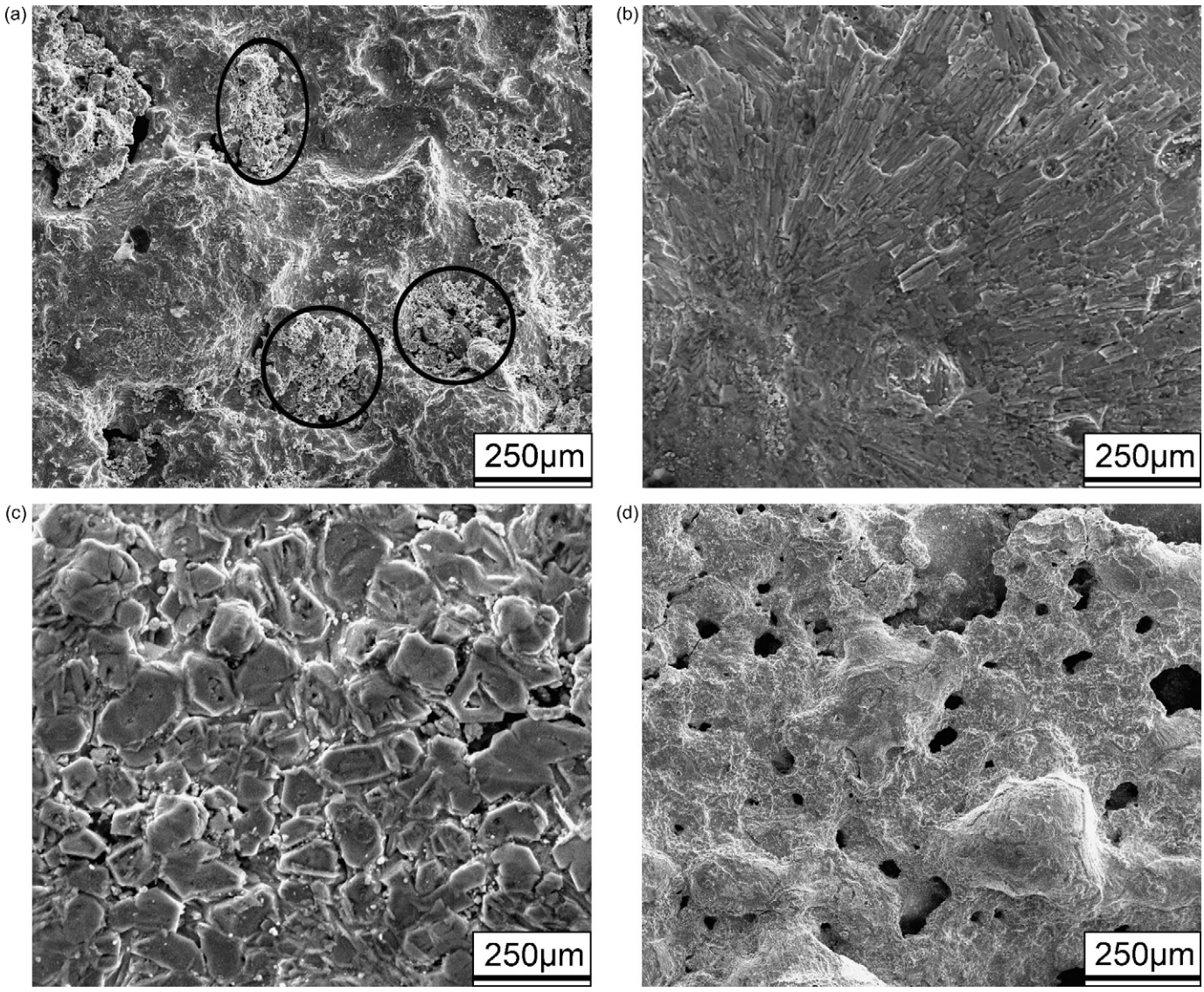

Fig. 3. SEM images showing typical surface morphologies of laser sintered samples prepared with selected parameters in different windows of Fig. 2: (a) 500 W, 0.04 m/s (point 1, zone I), (b) 700 W, 0.04 m/s (point 2, zone II), (c) 1000 W, 0.07 m/s (point 3, zone III), and (d) 1000 W, 0.05 m/s (point 4, zone IV). Fixed parameters are scan line spacing 0.15 mm and powder layer thickness 0.15 mm.

In spite of that, the four process windows can be used to choose the suitable processing conditions under which laser sintering will generate a feasible mechanism of melting.

The characteristic surface morphologies of laser sintered multi-layer samples obtained in the described windows are provided in Fig. 3. Table 1 depicts the statistics for the sintered densities using different sintering mechanisms. Laser sintering using parameters within zone I (point 1) produced a porous sintered surface containing some residual unsintered powder particles (circles denoted, Fig. 3a), resulting in a considerably low sintered density (Table 1). For point 2 within zone II, a relatively smooth and fully dense sintered surface was obtainable (Fig. 3b). Actually, the densification level of laser processed samples using parameters within zone II was generally higher than 92% theoretical density (TD). In the case of point 3 within zone III, the sintered surface consisted of rows of coarsened balls and interconnected inter-ball pore channels (Fig. 3c), leaving a high residual porosity (Table 1). More severely, balling effect, in most cases, handicapped the completion of a desired multi-layer sample, because balling phenomena made the smooth spreading of fresh power on the previously processed layer impossible, especially at the latter stage of sintering. As to point 4 within zone IV, a highly rippled surface consisting of large-sized pores was found (Fig. 3d). Besides the limited densification (Table 1), the sintered samples generally exhibited a significant geometric distortion (curling or delamination).

3.2. Microstructures

Although laser processing using the various parameters within zone II (Fig. 2) generally yielded a favorable densification (Table 1), the microstructural features on internal sections of laser sintered samples showed some pronounced differences, as revealed in Fig. 4. In general, the EDX analyses showed that the white phase was W, while the surrounding grey matrix was Cu. At a laser power of 600 W and a scan speed of 0.04 m/s (point 5), a heterogeneous microstructure consisting of clusters of W solids and irregular Cu-rich regions was visible (Fig. 4a). A high-magnified SEM image revealed that the fine W solids aggregated severely in the matrix (Fig. 4b). At a higher laser power of 700 W and the same scan speed (point 2), regular-shaped chain-like structures were present after

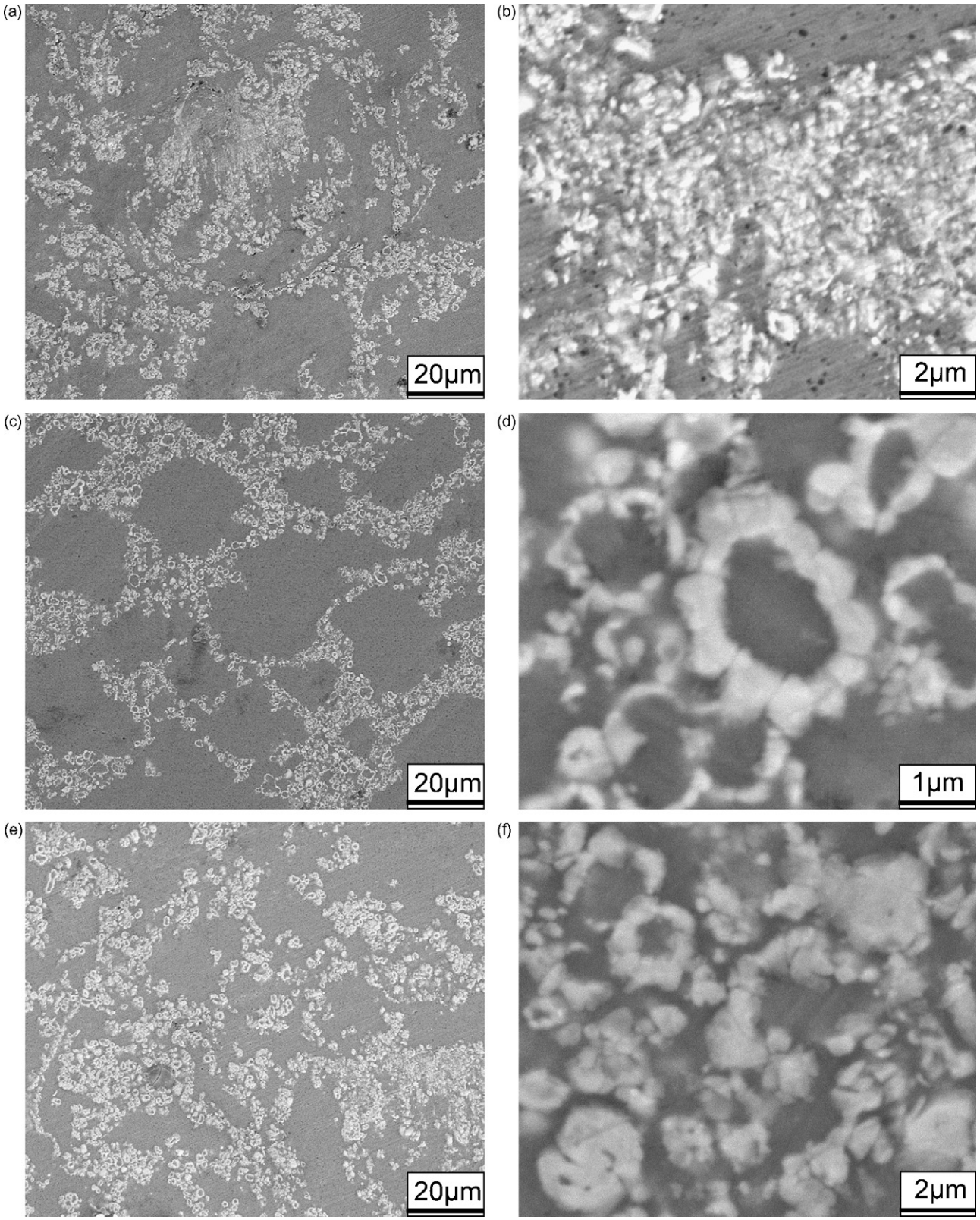

Fig. 4. SEM images showing characteristic microstructures on polished sections of laser sintered samples at different laser powers and scan speeds: (a) 600 W, 0.04 m/s (point 5, Fig. 2), (c) 700 W, 0.04 m/s (point 2), and (e) 850 W, 0.06 m/s (point 6). Fixed parameters are scan line spacing 0.15 mm and powder layer thickness 0.15 mm. (b), (d), and (f) are local magnifications of (a), (c), and (e), respectively.

Table 1
Average densification level of laser sintered multi-layer samples with various mechanisms of melting

Melting mechanism	Slight melting	Continuous melting	Melting with balling	Melting with breakage
Process window	Zone I	Zone II	Zone III	Zone IV
Densification level	<70% TD	>92% TD	<75% TD	~80% TD

sintering, showing a more homogeneous structure (Fig. 4c). More interestingly, the W solids were well arranged into a novel W-rim/Cu-core structure (Fig. 4d). However, at a higher scan speed of 0.06 m/s (point 6), the W solids again showed some aggregation in laser sintered matrix, thereby destroying such a W-rim/Cu-core structure (Fig. 4e and f).

Fig. 5 elucidates that the surface morphologies of laser sintered samples (e.g., size and shape of sintered agglomerates, amount of porosity) are strongly affected by scan line spacing. At a high scan line spacing of 0.30 mm (i.e., no overlap between scan lines), narrow columnar agglomerates parallel to the scan direction (arrowheaded) were formed, which were separated by large and interconnected gaps (Fig. 5a). As the spacing decreased to 0.25 mm (i.e., overlap between scan lines of 8.3%), the gaps between sintered agglomerates became shallow, although the surface was still rippled and rough (Fig. 5b). Interestingly, at an even lower spacing of 0.15 mm (i.e., overlap between scan lines of 25%), an almost fully dense and comparatively smooth surface was obtained (Fig. 5c).

In order to study the influence of layer thickness on sintering activity and densification response of the powder system, powder beds with various layer thicknesses were scanned at a fixed laser energy input, with the real-time sintering process illustrated in Fig. 6. The inter-layer bonding properties of the finished multi-layer samples are shown in Fig. 7. At a high layer thickness of 0.30 mm, a considerably large sparkle was observed in the laser irradiating region, resulting in a severe splash of the heated powder (Fig. 6a). In this situation, interconnected pore channels were present between sintered layers, resulting in a poor densification of

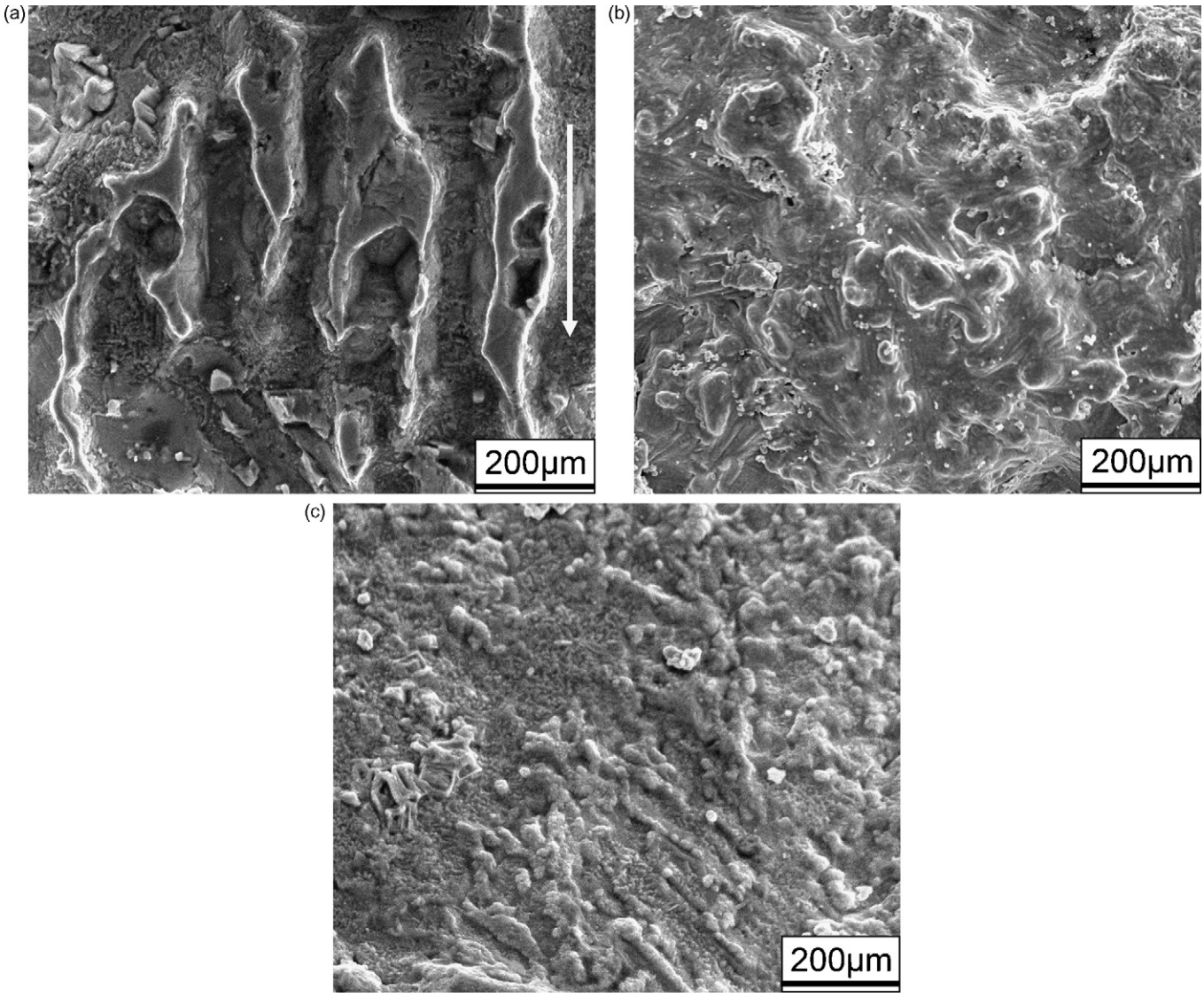

Fig. 5. SEM images showing typical surface morphologies of laser sintered samples with various scan line spacings: (a) 0.30 mm, (b) 0.25 mm, and (c) 0.15 mm. Fixed parameters are laser power 850 W, scan speed 0.05 m/s, and powder layer thickness 0.15 mm.

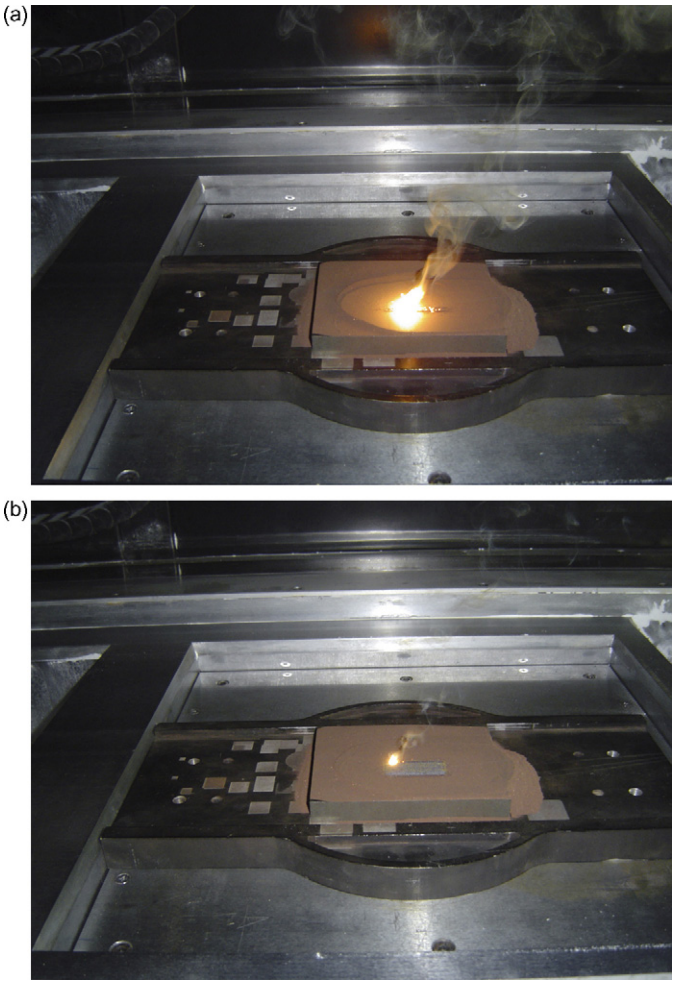

Fig. 6. Photographs of the real-time laser sintering process using different powder layer thicknesses: (a) 0.30 mm and (b) 0.15 mm.

78.3% TD (Fig. 7a). Differently, as decreasing the layer thickness to 0.15 mm, the powder was smoothly sintered without any apparent splash, exhibiting a small spark during powder-beam interaction (Fig. 6b). As a consequence, a sufficient densification (94.1% TD) combined with a favorable inter-layer bonding was obtained, showing no apparent pores or cracks between layers (Fig. 7b). However, it was noted that a further decrease in the layer thickness to 0.10 mm reduced the level of inter-layer microstructural homogeneity (Fig. 7c). The obtainable sintered density, 82.6% TD, also showed a decrease.

4. Discussion

4.1. Control of melting mechanisms by "linear energy density"

During DMLS, laser scanning is performed line-by-line over the powder bed at a constant speed. The dwelling time of the laser spot at any irradiating region is extremely short, typically less than 4 ms [10]. Due to such a localized nature of the rapid DMLS process, particle bonding must occur speedily, in the order of seconds [21]. Therefore, a sintering mechanism involving a liquid Cu phase is more reasonable for DMLS. Laser sintering of W–Cu system starts by means of the selective melting of Cu component, due to a significant difference in the melting temperatures of Cu and W (~1083 vs. ~3410 °C). A close look at the process map (Fig. 2) reveals that processing parameters are required to be carefully tailored, in order to achieve a favorable mechanism of melting. It is worthy noting that laser power (P) and scan speed (v) are the two main parameters involved in the individual line scanning. In order to assess their combined effect, a new concept, i.e., "linear energy density (LED)" (λ), is defined:

$$\lambda = \frac{P}{v} \quad (1)$$

After converting Fig. 2 into Fig. 8 using the defined LED, it is easy to find that the powder melting mechanisms show a distinct change with the incident LED. For a given LED below ~13 kJ/m, laser sintering at all scan speeds induces a considerably low degree of liquid formation due to an insufficient melting of the low melting point Cu component, which inevitably results in a large amount of residual porosity after sintering (Fig. 3a). Using a LED between ~13 and ~19 kJ/m proves to be feasible in realizing a continuous melting of the Cu component, thereby producing a sufficient amount of liquid phase. More molten liquid is thus likely to flow and infiltrate into the voids between the W solids, yielding a denser microstructure (Fig. 3b). However, using a high scan speed larger than 0.06 m/s incurs detrimental effects due to the occurrence of balling, even if the obtained LED falls within this favorable range (Fig. 3c). In this situation, the Cu liquid is able to spread around the W solid particles into a continuous film of a cylindrical shape in the initial stage of melting, owing to the sufficient energy input. However, due to an enhanced capillary instability effect induced by a higher scan speed, a significant transverse shrinkage distortion tends to initiate in inter-particle areas, resulting in the breakage of Cu liquid film along the molten track [22]. Also, a higher scan speed results in a rapid decrease in the diameter of the cylindrical shaped scan track. Thus, the radial contraction of the liquid track occurs, changing the direction of fluid flow from radially outward to radially inward and, eventually, causing the balling [23]. At an even higher LED above ~19 kJ/m, an excessive energy input enhances the operating temperature significantly, resulting in a high degree of superheating of the low melting phase Cu. The viscosity of liquid–solid mixture, thus, decreases markedly, which in turn elevates the Marangoni effect considerably. As a consequence, a significant shrinkage occurs during liquid–solid transition, thus decreasing the attainable density due to the formation of interrupted scan tracks and large-sized pores (Fig. 3d). Also, the overheating of the sintering system causes a large warping of the sintered parts owing to the high thermal gradients, which induce residual stresses relieved by shape change.

4.2. Influence of processing parameters on microstructures

It is well known that the conventional liquid phase sintering (LPS) process consists of three overlapping stages: particle rearrangement, solution reprecipitation, and solid-state sintering [15]. The W–Cu as investigated is a unique material combination because of the good wettability yet mutual insolubility of W in Cu, which makes the contribution of solution reprecipitation negligible [24,25]. Thus, only the first stage, i.e., particle rearrangement, plays a main role in realizing a successful DMLS due to the short interaction duration between the laser and the powder. In general, laser sintering using different LEDs within zone II of Fig. 8 yields a sound density (Table 1), which is mainly ascribed to the sufficient amount of liquid formation (Fig. 2). However, the microstructural homogeneity of DMLS-processed powder varies with the LED (Fig. 4). In detail, the LEDs corresponding to Fig. 4a, c, and e are 15, 17.5, and 14.2 kJ/m, respectively. Thus, it can be assumed that using a higher LED leads to a more homogeneous microstructure (Fig. 4c) combined with an interesting W-rim/Cu-core structure (Fig. 4d). A comparative study reveals that increasing laser power (Fig. 4a

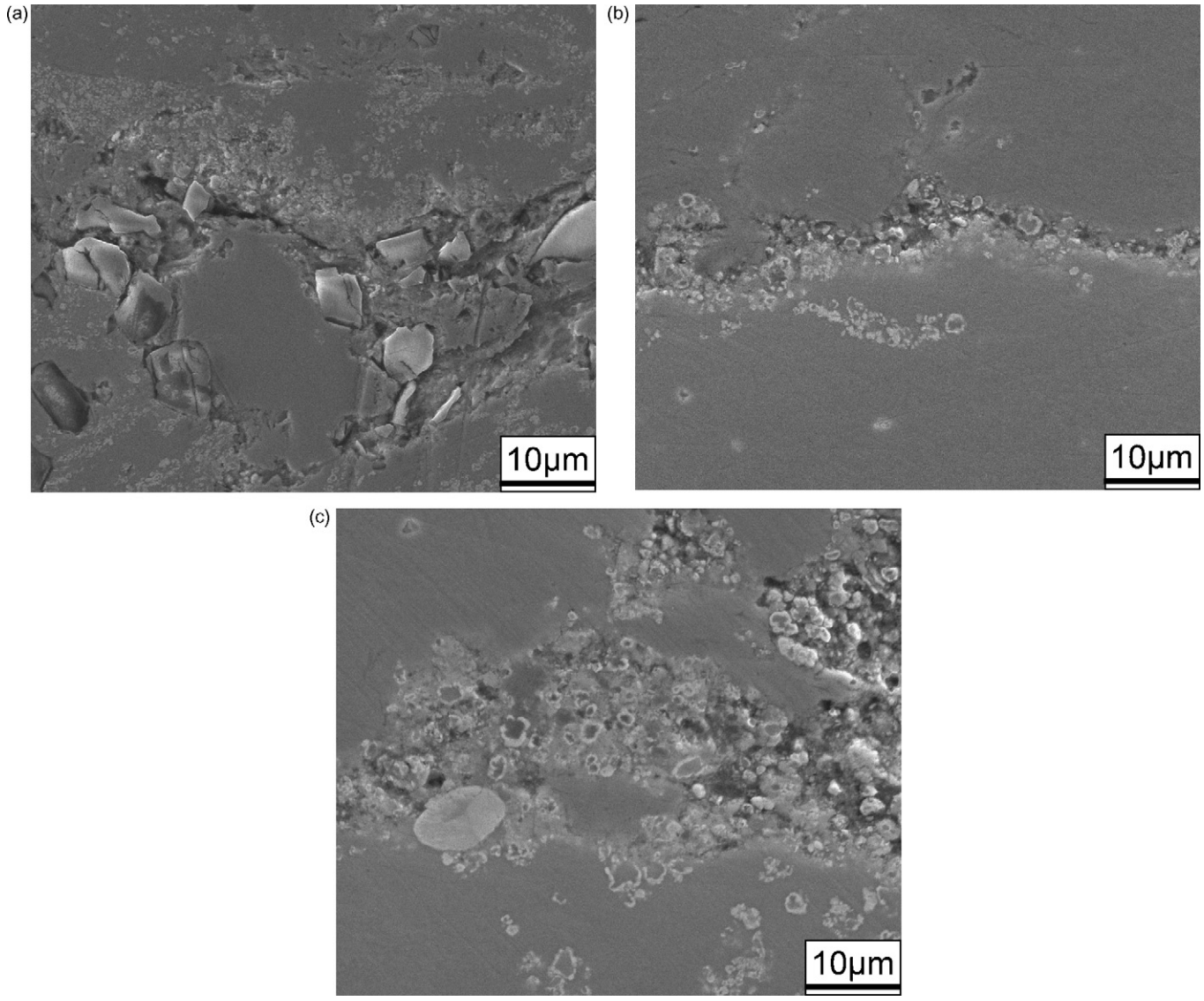

Fig. 7. SEM images on cross-sections of laser sintered samples showing inter-layer bonding at different layer thicknesses: (a) 0.30 mm, (b) 0.15 mm, and (c) 0.10 mm. Fixed parameters are laser power 850 W, scan speed 0.05 m/s, and scan line spacing 0.15 mm.

vs. Fig. 4c) or decreasing scan speed (Fig. 4e vs. Fig. 4c) can both enhance the LED. A higher LED, thus, favors a higher sintering temperature, due to a larger energy gain of the powder. It is known that the surface tension (σ, mN/m) of Cu liquid has a linear relationship with the temperature (T, °C), and can be estimated by [26]:

$$\sigma = 1330 - 0.23(T - 1085) \quad (2)$$

Therefore, a higher LED leads to a higher T and, accordingly, a lower σ. On the other hand, based on Takamichi and Roderick's results [27], the dynamic viscosity of the liquid (η, Pa·s) is defined by:

$$\eta = \frac{16}{15}\sqrt{\frac{m}{kT}}\sigma \quad (3)$$

where m is the atomic mass and k is the Boltzmann constant. From Eq. (3), one can notice that either a higher T or a lower σ leads to a smaller η. During DMLS of W–Cu composites, the main forces acting on W solids are: the capillary force for the rearrangement of W particles and the friction force due to the flow of Cu liquid around W particles [28]. Anestiev and Froyen's work [28] reveals that the capillary force is in inverse proportion to the σ, while the friction force

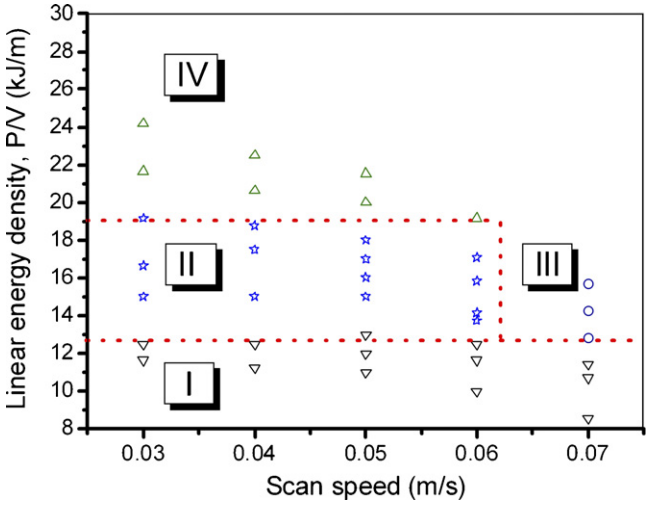

Fig. 8. Variation of powder melting mechanisms with linear energy density for the W–Cu system.

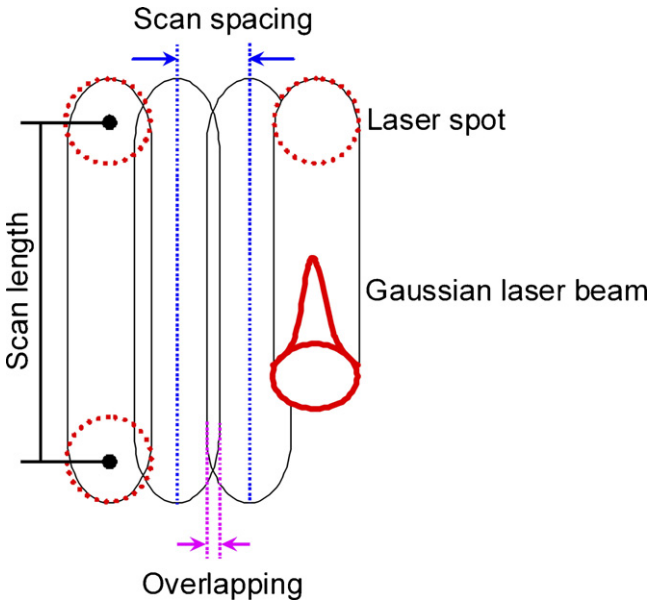

Fig. 9. Schematic of multi-line laser scanning.

is proportional to the η. Therefore, a decrease in σ and η (Eqs. (2) and (3)), which can be realized by increasing LED, enhances the capillary force and, meanwhile, lowers the friction force. The combined effect of these two factors favors the sufficient rearrangement of W particles, thus producing a homogeneous sintered structure free of the apparent aggregation of W solids (Fig. 4c). Additionally, an interesting W-rim/Cu-core structure is present in this situation (Fig. 4d). Our previous work [29] has proposed a reasonable mechanism for its formation, i.e, the combined action of the thermal Marangoni flow and the solutal one. Moreover, it shows that a decrease in the η leads to a stronger Marangoni flow [8], which favors the formation of such a novel structure.

On the other hand, the sintering and densification behavior in the W–Cu powder system would be influenced by scan line spacing during line-by-line laser melting (Fig. 5). As is evident from Niu and Chang's work [30], there exists a torque around the non-spherical W particles in Cu liquid, due to the misalignment of W solids. In addition, since the spatial intensity profile of the used laser beam follows a Gaussian distribution (Fig. 9), a large thermal gradient tends to develop between the centre and edge of the melt pool, which further gives rise to surface tension gradient and attendant Marangoni flow [31]. The combined effect of the present torque and Marangoni flow tends to rotate the W solids in the melt pool and, meanwhile, moves them towards the centre of the laser beam, where the temperature is the highest. As a consequence, arrays of agglomerates located at the centre of the scanned tracks and the large inter-track gaps are formed (Fig. 5a). Decreasing the scan line spacing brings the scan tracks closer to each other until they overlap (Fig. 9). The overlapping of the adjacent tracks makes it possible that a large part of the laser spot would scan over the previously scanned track and, accordingly, remelt the previously processed materials. This favors the flow and spreading of liquid between scan tracks and the escaping of some previously trapped air, leading to the enhancement of the inter-track bonding and the reduction in the sintered porosity (Fig. 5b and c).

The move to the fabrication of a multi-layer sample requires that an appropriate layer thickness to be determined. When the laser beam scans over the powder layer, the laser energy is directly absorbed by the solid particles through both, bulk coupling and powder coupling mechanisms [32]. Primarily, the laser energy is absorbed in a narrow layer of individual powder particles determined by the bulk properties of the materials, inducing a high temperature of the particle surface. The heat flows mainly towards the centre of the particles until a uniform temperature within the particles is obtained. Subsequently, the surrounding powder properties are responsible for the further thermal development. It is known that a large volume of gas phase exists in pores between particles. The heat conductivity of a loosely packed powder layer (k_p) can be described as [33]:

$$k_p = k_a \left(\frac{3}{\varphi_p} - 2 \right) \tag{4}$$

where k_a is the heat conductivity of the air and φ_p is the porosity of the powder layer. Eq. (4) reveals that the k_p is directly proportional to the k_a. Thus, at an initial stage of sintering the k_p is considerably low, since the k_a (0.0259 W/(m·K) at 20 °C and 1.01325×10^5 Pa) is negligible. Consequently, the heat generated during laser–powder interaction is difficult to conduct and transfer into the interior of the powder layer, especially for a thicker layer. The heat, thus, tends to accumulate on the surface of the layer, resulting in overheating and severe splashing of the powder (Fig. 6a). Also, interconnected pore channels between adjacent layers would be formed in this instance (Fig. 7a), since the powder layer has not been completely melted down due to the insufficient energy penetration. It is known that a certain portion of air in pores between particles tends to be trapped as bubbles during laser melting [34,35]. If the layer is thin, most bubbles, even at the bottom of the layer, are able to rise up to the surface of the layer and collapse, leading to less porosity. Furthermore, for a thinner layer, the laser energy can not only completely penetrate the current layer, but also remelt the surface of the previously sintered layer, thus obtaining coherently bonded layers (Fig. 7b). However, for a given laser energy, a further decrease in layer thickness would result in an excessive liquid formation via overmuch remelting of the previously processed materials, thus greatly enhancing the Marangoni effect. The elevated Marangoni forces would roughen the sintered surface, producing a considerably heterogeneous inter-layer microstructure (Fig. 7c).

4.3. Integrated process control using "volumetric energy density"

DMLS is a complicated free-form shaping process, which follows a processing routine from a "line" to a "layer" and, subsequently, to a "bulk". DMLS starts with a single line scanning, thus introducing two main parameters, i.e., laser power (P) and scan speed (v). The completion of multiple scan lines leads to the formation of a sintered layer. Here, another parameter, i.e., scan line spacing (h), is involved. The layer-by-layer bonding and consolidation yields a bulk component, which requires a suitable powder layer thickness (d) to be determined. In light of the experimental results, as listed in Section 3, it is clear that the P, v, h, and d all have great influence on the densification and attendant microstructural features of DMLS-processed W–Cu composites. In order to evaluate the combined effect of these parameters and, thus, control the DMLS process integrally, besides the above-proposed LED, another single factor termed "volumetric energy density (VED)" (ε) is defined as follows:

$$\varepsilon = \frac{P}{vhd} \tag{5}$$

The unit of VED is kJ/mm^3. Fig. 10 depicts the relationship between the laser sintered density and the VED under different processing conditions. It is evident that for a given VED between ~0.6 and ~0.8 kJ/mm^3, the attainable density is generally high (>90% TD). Either a VED below ~0.6 kJ/mm^3 or a VED above ~0.8 kJ/mm^3

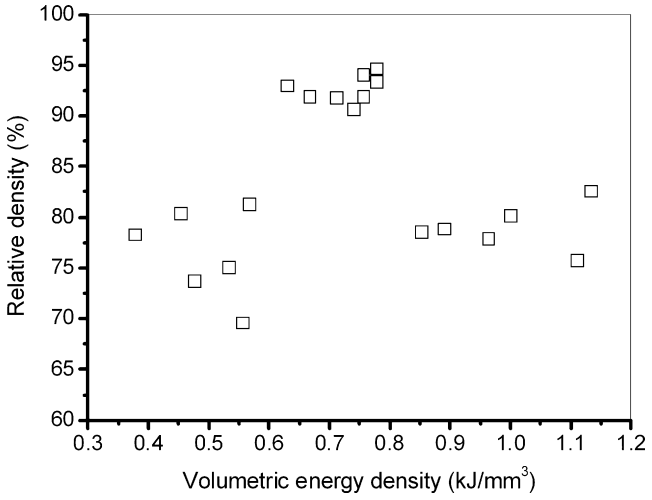

Fig. 10. Change of relative density of laser sintered samples with volumetric energy density for the W–Cu system. Only valid between 0.02 and 0.06 m/s scan speed.

results in a poor densification. For example, the surface morphologies of laser sintered samples at the VEDs of 0.556, 0.756, and 0.889 kJ/mm^3 are shown in Figs. 3a, 5c, and 3d, respectively. Here, it should be noted that although a suitable VED can be obtained by using a high laser power combined with a high scan speed, balling phenomena would initiate under such a condition (Figs. 2 and 8), which ultimately deteriorates the densification level. For instance, the VED corresponding to Fig. 3c (i.e., 0.635 kJ/mm^3) falls within the above favorable range, but a higher scan speed in this case (i.e., 0.07 m/s) causes the balling and resultant porosity.

5. Conclusions

The processing conditions and control methods for direct laser sintering of submicron W–Cu/ micron Cu powder system are investigated, and the following conclusions can be drawn.

(1) A linear energy density between ~13 and ~19 kJ/m combined with a suitable scan speed (<0.06 m/s) leads to a continuous melting of the Cu component, yielding a sound densification level (>92% theoretical density) free of any balling phenomena.
(2) A proper increase in the linear energy density above ~13 kJ/m, which is realized by increasing laser power or lowering scan speed, improves the microstructural homogeneity of laser sintered materials.
(3) Narrowing the scan line spacing to 0.15 mm is able to enhance the inter-track bonding, and to reduce the roughness of the laser sintered surface.
(4) Decreasing the powder layer thickness to 0.15 mm is a promising approach for improving the bonding ability between sintered layers. A further decrease in the layer thickness to 0.10 mm produces a heterogeneous inter-layer microstructure.
(5) Setting the volumetric energy density within ~0.6 and ~0.8 kJ/mm^3 facilitates an integrated control of the laser sintering process, which proves to be an efficient method to produce high-density sintered parts.

Acknowledgements

The authors thank the financial support from the National Natural Science Foundation of China (Grant No. 50775113). One of the authors (Dongdong Gu) gratefully appreciates the financial support from the Scientific Research Foundation for Newly Employed Talents in Nanjing University of Aeronautics and Astronautics.

References

[1] I. Smid, Mater. Sci. Forum 475–479 (2005) 1355–1360.
[2] G. Pintsuk, I. Smid, J.E. Döring, W. Hohenauer, J. Linke, J. Mater. Sci. 42 (2007) 30–39.
[3] G. Pintsuk, S.E. Brünings, J.E. Döring, J. Linke, I. Smid, L. Xue, Fusion Eng. Des. 66–68 (2003) 237–240.
[4] M.H. Maneshian, A. Simchi, Z.R. Hesabi, Mater. Sci. Eng. A 445–446 (2007) 86–93.
[5] M.H. Maneshian, A. Simchi, J. Alloys Compd. 463 (2008) 153–159.
[6] F.A. da Costa, A.G.P. da Silva, U.U. Gomes, Powder Technol. 134 (2003) 123–132.
[7] M. Rosinski, E. Fortuna, A. Michalski, Z. Pakiela, K.J. Kurzydlowski, Fusion Eng. Des. 82 (2007) 2621–2626.
[8] D.D. Gu, Y.F. Shen, Mater. Sci. Eng. A 489 (2008) 169–177.
[9] A. Simchi, F. Petzoldt, H. Pohl, J. Mater. Process. Technol. 141 (2003) 319–328.
[10] A. Simchi, H. Pohl, Mater. Sci. Eng. A 359 (2003) 119–128.
[11] A. Simchi, H. Pohl, Mater. Sci. Eng. A 383 (2004) 191–200.
[12] A. Simchi, Mater. Sci. Eng. A 428 (2006) 148–158.
[13] A. Simchi, Mater. Lett. 62 (2008) 2840–2843.
[14] J.P. Kruth, G. Levy, F. Klocke, T.H.C. Childs, CIRP Ann. Manuf. Technol. 56 (2007) 730–759.
[15] H.H. Zhu, L. Lu, J.Y.H. Fuh, Mater. Sci. Eng. A 371 (2004) 170–177.
[16] S. Das, Adv. Eng. Mater. 5 (2003) 701–711.
[17] A. Simchi, F. Petzoldt, H. Pohl, Int. J. Powder Metall. 37 (2001) 49–61.
[18] M.C. Yang, Z.Z. Song, K. Lu, Acta Metall. Sin. 40 (2004) 639–642.
[19] D.D. Gu, Y.F. Shen, Mater. Sci. Eng. A 435–436 (2006) 54–61.
[20] D.D. Gu, Y.F. Shen, S.Q. Fang, J. Xiao, J. Alloys Compd. 438 (2007) 184–189.
[21] M. Agarwala, D. Bourell, J. Beaman, H. Marcus, J. Barlow, Rapid Prototyping J. 1 (1995) 26–36.
[22] D.D. Gu, Y.F. Shen, J. Alloys Compd. 432 (2007) 163–166.
[23] H.J. Niu, I.T.H. Chang, Scripta Mater. 41 (1999) 1229–1234.
[24] J.L. Johnson, J.J. Brezovsky, R.M. German, Metall. Mater. Trans. A 36 (2005) 1557–1565.
[25] J.L. Johnson, J.J. Brezovsky, R.M. German, Metall. Mater. Trans. A 36 (2005) 2807–2814.
[26] Z.F. Yuan, J.J. Ke, J. Li, Surface Tension of Metals and Alloys, first ed., Science Press, Beijing, 2006.
[27] I. Takamichi, I.L.G. Roderick, The Physical Properties of Liquid Metals, first ed., Clarendon Press, Oxford, 1993.
[28] L.A. Anestiev, L. Froyen, J. Appl. Phys. 86 (1999) 4008–4017.
[29] D.D. Gu, Y.F. Shen, X.J. Wu, Mater. Lett. 62 (2008) 1765–1768.
[30] H.J. Niu, I.T.H. Chang, Scripta Mater. 41 (1999) 25–30.
[31] C. Lampa, A.F.H. Kaplan, M. Resch, C. Magnusson, Laser Eng. 7 (1998) 241–252.
[32] P. Fischer, V. Romano, H.P. Weber, N.P. Karapatis, E. Boillat, R. Glardon, Acta Mater. 51 (2003) 1651–1662.
[33] D.D. Gu, Y.F. Shen, M.C. Liu, Y.F. Pan, C.T. Xu, Trans. Nanjing Univ. Aeronaut. Astronaut. 21 (2004) 225–233.
[34] A.N. Chatterjee, S. Kumar, P. Saha, P.K. Mishra, A.R. Choudhury, J. Mater. Process. Technol. 136 (2003) 151–157.
[35] S. Dingal, T.R. Pradhan, J.K.S. Sundar, A.R. Choudhury, S.K. Roy, Int. J. Adv. Manuf. Technol. (2007), doi:10.1007/s00170-007-1154-1.